Chapter 8

Coherent backscattering of light

8.1 Introduction

Phase coherence is at the basis of the interference effects which lead to weak localization in electronics. This phase coherence has also important consequences in optics. Moreover, using an incident laser beam, it is possible in optics to study the angular behavior of both transmitted and reflected waves. This is difficult in electronic devices, where electrons are injected and collected from reservoirs and do not have an accessible angular structure. In this chapter, we study the intensity of the light reflected by a diffusive medium and we show that it has an angular structure that is due to the coherent effects associated with the Cooperon. We also show that it is possible to single out and analyze the contribution of multiple scattering paths as a function of their length. This leads to a kind of "spectroscopy" of diffusive trajectories.

The issue of wave scattering in disordered media has a long history. At the turn of the twentieth century, a purely classical approach to the description of radiative transfer of electromagnetic waves through the atmosphere, based on the Boltzmann equation, had already been proposed by Schuster [200]. This problem was subsequently extended to include the related domains of turbulent media, meteorology and liquids. It was only during the 1980s, however, that the possibility of phase coherent effects in the multiple scattering of waves in random media was raised. The interest surrounding this question is certainly related to new developments obtained on similar questions in the quantum theory of scattering [201, 202, 203]. A systematic description of coherent effects emphasizing the role of the Cooperon was initially proposed in references [204] and [205]. These new developments came together with the first experimental results [206, 207, 208], giving rise to a large number of works which it would be rather difficult to list comprehensively [209]; we shall quote only a few in this chapter. Nevertheless, we follow here the approach developed in references

[210, 211, 212] [1].

The variety of phenomena that result from multiple scattering of electromagnetic waves is rather broad. Consequently, the coherent backscattering phenomenon that we study in this chapter has a large range of applications that have been developed only during the last few years. We shall not study them all, but rather present some of them towards the end of this chapter.

We consider first the case of a scalar wave, and then we include effects of polarization. We define and study the reflection coefficient (sometimes called the *albedo*) of a semi-infinite diffusive medium in terms of the Diffuson and of the Cooperon. We then extend those results to the case of a finite absorption. Finally, we present a rather detailed account of the experimental situation which shows quite spectacularly the success of the present ideas about coherent multiple scattering and its large field of applicability.

8.2 The geometry of the albedo

8.2.1 Definition

The physical situation we aim to describe is as follows. A far-field and point-like source emits a monochromatic light which we assimilate to a plane wave directed towards the interface between vacuum and the diffusive medium. The direction of this plane wave is characterized by the unit vector $\hat{\boldsymbol{s}}_i$. The wave scattered by the medium emerges through the same interface (*i.e.*, in reflection) and is detected far from the interface along the direction $\hat{\boldsymbol{s}}_e$. We are thus interested in the angular dependence of the reflection coefficient called *albedo* (it is also sometimes called *bistatic coefficient* [213, 214]). There are several definitions of this coefficient which are appropriate to different fields of physics such as astrophysics, atomic physics, nuclear physics, etc. For instance, in astronomy, the albedo of planets is defined as the ratio between the total reflected light flux and the incident flux coming from the Sun. Thus defined, the albedo of the Earth is 35% while that of the Moon is only 6%. For more details, see references [213, 214].

The detector of the outgoing light along the direction $\hat{\boldsymbol{s}}_e$ essentially measures the intensity $I(R\hat{\boldsymbol{s}}_e) \propto E^2$ of the electromagnetic field $E(R\hat{\boldsymbol{s}}_e)$. For a spherical wave detected at a distance R which is large compared to the size of the interface, the energy flux per unit time and per unit solid angle is

$$\frac{dF}{d\Omega} = cR^2 I(R\hat{\boldsymbol{s}}_e) \quad , \tag{8.1}$$

where F is the flux of the Poynting vector. The incident flux is given by [2]

$$F_0 = cSI_0 \quad , \tag{8.2}$$

[1] This choice of references should not be understood as resulting from a formed opinion on other references. Its aim is simply to use those references whose notations are close to those used in this book.

[2] We consider here the situation of a normal incidence. In the general case, the incident flux depends on the cosine of the angle between the incident direction and the perpendicular to the surface.

and we define the albedo $\alpha(\hat{\boldsymbol{s}}_e)$ by the dimensionless ratio

$$\boxed{\alpha(\hat{\boldsymbol{s}}_e) = \frac{1}{F_0}\frac{dF}{d\Omega} = \frac{R^2}{S}\frac{I(R\hat{\boldsymbol{s}}_e)}{I_0}} \tag{8.3}$$

The albedo appears to be a quantity close to a differential cross section (see also the relation 2.66) up to a multiplicative factor related to the shape of the interface of the diffusive medium.

8.2.2 Albedo of a diffusive medium

The albedo characterizes the light scattered by a diffusive medium. To calculate this quantity, we need to evaluate the intensity $I(R\hat{\boldsymbol{s}}_e)$ of the scattered field as defined by relation (4.54) [3]. We start by presenting a heuristic derivation that allows us to calculate the Diffuson and Cooperon contributions and to understand the characteristics of the coherent albedo (triangular singularity, algebraic decrease etc.).

We consider a semi-infinite diffusive medium filling the half-space $z \geq 0$. The half-space $z \leq 0$ is a free space that contains the source and the detectors (Fig. 8.1). The incident (assumed to be normal to the interface) and emergent beams are respectively characterized by the wave vectors $\boldsymbol{k}_i = k\hat{\boldsymbol{s}}_i$ and $\boldsymbol{k}_e = k\hat{\boldsymbol{s}}_e$ where $\hat{\boldsymbol{s}}_i$ and $\hat{\boldsymbol{s}}_e$ are unit vectors. Since the waves experience elastic scattering, only their direction $\hat{\boldsymbol{s}}$ changes while the amplitude $k = \omega_0/c$ remains constant. Moreover, we also assume that the difference in optical index between the two media is negligible.

In order to calculate the intensity $I(R\hat{\boldsymbol{s}}_e)$, we first consider the case of a scalar wave solution of the Helmholtz equation (2.8). This solution corresponds to an incident plane wave and to a spherical outgoing wave detected at a point $\boldsymbol{R} = R\hat{\boldsymbol{s}}_e$ in the far field, namely at a distance which is very large compared to the size of the interface of the diffusive medium (Figure 8.1). For a given incident direction $\hat{\boldsymbol{s}}_i$, the amplitude $\psi_{\omega_0}(\hat{\boldsymbol{s}}_e)$ of the outgoing wave has the following structure

$$\psi_{\omega_0}(\hat{\boldsymbol{s}}_e) \propto \int d\boldsymbol{r}d\boldsymbol{r}' e^{ik(\hat{\boldsymbol{s}}_i.\boldsymbol{r}-\hat{\boldsymbol{s}}_e.\boldsymbol{r}')} G(\boldsymbol{r},\boldsymbol{r}',\omega_0) \quad . \tag{8.4}$$

This expression is nothing but the Fourier transform of the Green's function (4.21), and it has the form

$$\psi_{\omega_0}(\hat{\boldsymbol{s}}_e) = \int d\boldsymbol{r}d\boldsymbol{r}' e^{ik(\hat{\boldsymbol{s}}_i.\boldsymbol{r}-\hat{\boldsymbol{s}}_e.\boldsymbol{r}')} \sum_{N=1}^{\infty} \sum_{\boldsymbol{r}_1,\cdots,\boldsymbol{r}_N} |A(\boldsymbol{r},\boldsymbol{r}',\mathcal{C}_N)| \exp(i\frac{2\pi\mathcal{L}_N}{\lambda}) \tag{8.5}$$

and the intensity is $I(R\hat{\boldsymbol{s}}_e) = \frac{4\pi}{c}|\psi_{\omega_0}(\hat{\boldsymbol{s}}_e)|^2$. In this expression the points $\boldsymbol{r}$ and $\boldsymbol{r}'$ can be anywhere on the interface, whereas the points $\boldsymbol{r}_i$ correspond to

[3] In the definition (4.54) the source of the field is a δ function of unit strength so that the intensity thus defined does not have the dimensions of a light intensity. This is not very important since the albedo appears as the ratio of two such intensities.

scattering events. $\mathcal{C}_N = (\boldsymbol{r}_1, \boldsymbol{r}_2, ..., \boldsymbol{r}_N)$ is a sequence of N scattering events and $\mathcal{L}_N/\lambda$ is the total length of the corresponding trajectory measured in units of the wavelength $\lambda = \frac{2\pi}{k}$. The field ψ_{ω_0} thus appears as a sum over all the possible multiple scattering sequences in the half-space $z \geq 0$, weighted by the phase factors that account for the two incident and emergent waves in the free half-space $z \leq 0$.

There are three distinct contributions to the albedo α. The first includes all the terms for which the sequences that contribute respectively to ψ_{ω_0} and $\psi^*_{\omega_0}$ are different (as represented in Figure 4.1). The second contribution includes all the terms that correspond to identical scattering sequences (Figure 8.1). The third and last contribution corresponds also to identical scattering sequences propagating in opposite directions (Figure 8.2).

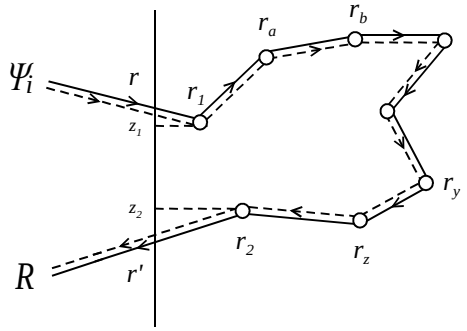

Figure 8.1: *Contribution of the Diffuson to the albedo averaged over disorder. We have assumed in the calculation that the incident beam is perpendicular to the interface.*

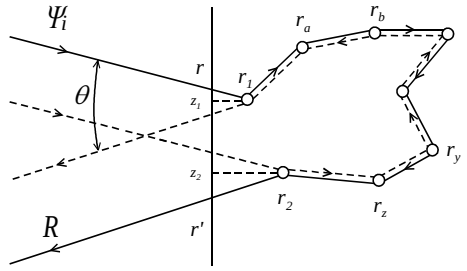

Figure 8.2: *Contribution of the Cooperon to the albedo averaged over disorder. We have assumed in the calculation that the incident beam is perpendicular to the interface.*

For a given realization of the disorder, *i.e.*, of the position of the scatterers, the first term provides the main contribution α_s to the albedo, but vanishes upon disorder averaging (Fig. 1.4). This term corresponds to the fluctuations or speckle patterns that we shall study in Chapter 12. The two remaining contributions denoted α_d and α_c have a finite average value and correspond

respectively to the Diffuson and the Cooperon, namely to the incoherent and coherent parts.

8.3 The average albedo

8.3.1 Incoherent albedo : contribution of the Diffuson

As stated before, the only multiple scattering trajectories that still contribute to disorder averaging are those for which the sequences $\mathcal{C}_N$ of scattering events that enter the amplitudes ψ_{ω_0} and $\psi^*_{\omega_0}$ are identical. In order to derive an expression for the average albedo, we need to evaluate at the approximation of the Diffuson the reflected average intensity, $I_d(R\hat{\boldsymbol{s}}_e)$ at a point $\boldsymbol{R} = R\hat{\boldsymbol{s}}_e$ at infinity.

In the experimental setup for the albedo measurement, both the source and the detector are placed *outside* the diffusive medium so that we must also include the conversion of the incident plane wave into a diffusing wave and of the diffusing wave back into an outgoing spherical wave. Several approaches are thus possible. The most natural is to proceed as in Chapter 4, namely to describe multiple scattering as a product $\overline{G}\ \overline{G}\ \Gamma\ \overline{G}\ \overline{G}$ (see relations 4.37 or 4.60), where $\overline{G}$ is an average Green's function and where Γ is the structure factor [4] of the Diffuson. We thus obtain an expression analogous to (4.60) which takes the form,

$$I_d(R\hat{\boldsymbol{s}}_e) = \frac{4\pi}{c}\int d\boldsymbol{r}_1 d\boldsymbol{r}_2 |\overline{\psi}_i(\boldsymbol{r}_1)|^2 |\Gamma(\boldsymbol{r}_1,\boldsymbol{r}_2)|\overline{G}^R(\boldsymbol{r}_2,\boldsymbol{R})|^2 \quad . \tag{8.6}$$

The structure of this expression is represented in Figure 8.1. $|\overline{\psi}_i(\boldsymbol{r}_1)|^2$ is the average intensity at point $\boldsymbol{r}_1$ that originates directly from the light source, *i.e.*, without intermediate scattering. It can thus be calculated within the Drude-Boltzmann approximation. The term $|\overline{G}^R(\boldsymbol{r}_2,\boldsymbol{R})|^2$ describes, at the same approximation, the wave propagation between the last scattering event in $\boldsymbol{r}_2$ and any point $\boldsymbol{R}$. Finally, $\Gamma(\boldsymbol{r}_1,\boldsymbol{r}_2)$ is the Diffuson structure factor, which obeys equation (4.24).

For the geometry that we are considering, the source term is well described by an incident plane wave so that

$$\overline{\psi}_i(\boldsymbol{r}_1) = \sqrt{\frac{cI_0}{4\pi}} e^{-|\boldsymbol{r}_1-\boldsymbol{r}|/2l_e} e^{-ik\hat{\boldsymbol{s}}_i.\boldsymbol{r}_1} \quad , \tag{8.7}$$

in which $\boldsymbol{r}$ is the intersection of the incident beam with the interface placed at $z = 0$, $\boldsymbol{r}_1$ is the location of the first scattering event, and $k\hat{\boldsymbol{s}}_i$ is the wave vector of the incident plane wave (Figure 8.1). The average albedo at the Diffuson approximation is obtained from the relations (8.3) and (8.6) and it takes the form

$$\alpha_d = \frac{R^2}{S}\int d\boldsymbol{r}_1 d\boldsymbol{r}_2 e^{-|\boldsymbol{r}_1-\boldsymbol{r}|/l_e} \Gamma(\boldsymbol{r}_1,\boldsymbol{r}_2)|\overline{G}^R(\boldsymbol{r}_2,\boldsymbol{R})|^2 \quad . \tag{8.8}$$

[4] From now on, we shall no longer specify the frequency ω_0 of the waves.

For $|\boldsymbol{R}-\boldsymbol{r}_2| \to \infty$ (Fraunhoffer approximation), the average Green's function $\overline{G}^R(\boldsymbol{r}_2,\boldsymbol{R})$ given by relation (3.48) can be expanded as (see 2.56) :

$$\begin{aligned}\overline{G}^R(\boldsymbol{r}_2,\boldsymbol{R}) &= e^{-|\boldsymbol{r}'-\boldsymbol{r}_2|/2l_e}\frac{e^{ik|\boldsymbol{R}-\boldsymbol{r}_2|}}{4\pi|\boldsymbol{R}-\boldsymbol{r}_2|} \\ &\simeq e^{-|\boldsymbol{r}'-\boldsymbol{r}_2|/2l_e}e^{-ik\hat{\boldsymbol{s}}_e.\boldsymbol{r}_2}\frac{e^{-ikR}}{4\pi R} \quad . \end{aligned} \tag{8.9}$$

Introducing the projection [5] μ of the unit vector $\hat{\boldsymbol{s}}_e$ on the Oz-axis, we obtain $|\boldsymbol{r}_2-\boldsymbol{r}'| = z_2/\mu$ and $|\boldsymbol{r}_1-\boldsymbol{r}| = z_1$ so that the expression of the incoherent albedo associated to the Diffuson finally takes the form

$$\boxed{\alpha_d = \frac{1}{(4\pi)^2 S}\int d\boldsymbol{r}_1 d\boldsymbol{r}_2 e^{-\frac{z_1}{l_e}}e^{-\frac{z_2}{\mu l_e}}\Gamma(\boldsymbol{r}_1,\boldsymbol{r}_2)} \tag{8.10}$$

Moreover, by assuming slow spatial variations, the structure factor $\Gamma(\boldsymbol{r}_1,\boldsymbol{r}_2)$, solution of equation (4.26), is shown to obey the diffusion equation

$$-D\Delta_{\boldsymbol{r}_2}\Gamma(\boldsymbol{r}_1,\boldsymbol{r}_2) = \frac{4\pi c}{l_e^2}\delta(\boldsymbol{r}_1-\boldsymbol{r}_2) \tag{8.11}$$

and it is related to the probability $P_d(\boldsymbol{r}_1,\boldsymbol{r}_2)$ through the relation (4.63) :

$$P_d(\boldsymbol{r}_1,\boldsymbol{r}_2) = \frac{l_e^2}{4\pi c}\Gamma(\boldsymbol{r}_1,\boldsymbol{r}_2) \quad . \tag{8.12}$$

Inserting this relation into (8.10), we obtain

$$\boxed{\alpha_d = \frac{c}{4\pi l_e^2}\int_0^\infty dz_1 dz_2 e^{-\frac{z_1}{l_e}}e^{-\frac{z_2}{\mu l_e}}P_d(z_1,z_2)} \tag{8.13}$$

with $P_d(z_1,z_2) = \int_S d^2\boldsymbol{\rho}\, P_d(\boldsymbol{\rho},z_1,z_2)$. For the geometry of a semi-infinite medium, the function $P_d(\boldsymbol{\rho},z_1,z_2)$ depends on the coordinates z_1 and z_2 as well as on the projection $\boldsymbol{\rho}$ of the vector $\boldsymbol{r}_1-\boldsymbol{r}_2$ on the plane $z=0$.

The calculation of the average albedo thus reduces to that of the probability P_d in a semi-infinite medium. We have shown (section A5.2.3) that, for this geometry, P_d is well described by the solution of a diffusion equation, provided we choose as an effective boundary condition that P_d vanishes at the point $-z_0$ with $z_0 = \frac{2}{3}l_e$ [215] [6]. The solution of the corresponding stationary diffusion equation is obtained using the image method (section 5.7 and Appendix A5.3).

[5] We assume that the incident beam is perpendicular to the interface.

[6] The exact solution of the Milne problem (Appendix A5.3) gives $z_0 \simeq 0.710\, l_e$. But this value is not consistent with the diffusion approximation. We shall thus consider instead the value $z_0 = 2/3l_e$ obtained within this approximation.

The images of the points $\boldsymbol{r}_1$ and $\boldsymbol{r}_2$ are determined with respect to the plane $-z_0$, so that the probability $P_d(\boldsymbol{\rho}, z_1, z_2)$ becomes

$$P_d(\boldsymbol{\rho}, z_1, z_2) = \frac{1}{4\pi D}\left(\frac{1}{\sqrt{\rho^2+(z_1-z_2)^2}} - \frac{1}{\sqrt{\rho^2+(z_1+z_2+2z_0)^2}}\right) . \quad (8.14)$$

The integration over $\boldsymbol{\rho}$ leads to (relation 5.156)

$$P_d(z_1, z_2) = \frac{1}{2D}\left[(z_1+z_2+2z_0) - |z_1-z_2|\right] = \frac{z_m+z_0}{D} \quad (8.15)$$

where $z_m = \min(z_1, z_2)$. Using (8.13), we finally obtain for the albedo α_d the expression

$$\boxed{\alpha_d = \frac{3}{4\pi}\mu\left(\frac{z_0}{l_e} + \frac{\mu}{\mu+1}\right)} \quad (8.16)$$

From this relation, it appears that within the Diffuson approximation the average albedo of an optically thick medium is almost independent of the angle between the incident beam and the direction $\hat{\boldsymbol{s}}_e$ of the outgoing wave (see Figure 8.7).

Remarks

- The previous expression for α_d results from the calculation of the intensity $I_d(\boldsymbol{R})$ at a point outside the diffusive medium. This is an approximation. The theory of radiative transfer (Appendix A5.2) amounts to calculating the specific intensity $I_d(z=0, \hat{\boldsymbol{s}}_e)$ at the interface along a given outgoing direction $\hat{\boldsymbol{s}}_e$ (5.131). This approach leads to a different expression of the albedo, namely,

$$\alpha_d = \frac{3}{4\pi}\mu\left(\frac{z_0}{l_e} + \mu\right) \quad (8.17)$$

  which, in contrast to (8.16), is normalized, $2\pi\int_0^{\pi/2}\alpha_d(\theta)\sin\theta d\theta = 1$. Nevertheless, we have chosen here to present the simplest derivation. It will be useful to get some intuition about the angular dependence of the coherent albedo and of the coherent backscattering cone.

- At first glance, the previous derivation of the average albedo does apply to isotropic scatterers only, *i.e.*, for a transport mean free path l^* equal to l_e. For the case of anisotropic scattering, the angular dependence of the structure factor should be taken into account (Appendix A4.3). The albedo α_d becomes

$$\alpha_d = \frac{1}{(4\pi)^2 S}\int d\boldsymbol{r}_1 d\boldsymbol{r}_2 e^{-\frac{z_1}{l_e}} e^{-\frac{z_2}{\mu l_e}} \Gamma(\hat{\boldsymbol{s}}_i, \hat{\boldsymbol{s}}_e, \boldsymbol{r}_1, \boldsymbol{r}_2) \quad (8.18)$$

  where $\Gamma(\hat{\boldsymbol{s}}_i, \hat{\boldsymbol{s}}_e, \boldsymbol{r}_1, \boldsymbol{r}_2)$ is the Fourier transform of $\Gamma(\hat{\boldsymbol{s}}_i, \hat{\boldsymbol{s}}_e, \boldsymbol{q})$ defined by (4.156). We shall return to this point in section 8.6.

8.3.2 The coherent albedo : contribution of the Cooperon

We consider now the contribution α_c of the Cooperon to the average albedo as represented in Figure 8.2. As for the incoherent contribution, we describe the conversion of a plane wave into a diffusing wave by means of an average Green's function that decreases exponentially while entering the diffusive medium. The intensity $I_c(R\hat{\boldsymbol{s}}_e)$ is given by the relation (4.61), namely,

$$I_c(R\hat{\boldsymbol{s}}_e) = \frac{4\pi}{c}\int d\boldsymbol{r}_1 d\boldsymbol{r}_2 \overline{\psi}_i(\boldsymbol{r}_1)\overline{\psi}_i{}^*(\boldsymbol{r}_2)\Gamma'(\boldsymbol{r}_1,\boldsymbol{r}_2)\overline{G}^R(\boldsymbol{r}_2,\boldsymbol{R})\overline{G}^A(\boldsymbol{R},\boldsymbol{r}_1) \quad (8.19)$$

where $\Gamma'(\boldsymbol{r}_1,\boldsymbol{r}_2)$ is the Cooperon structure factor (section 4.6). Time reversal invariance implies that $\Gamma' = \Gamma$. Considering as previously an incident plane wave (8.7) and using the Fraunhoffer approximation (8.9) for the Green's functions, we obtain

$$\begin{aligned}\alpha_c &= \frac{R^2}{S}\int d\boldsymbol{r}_1 d\boldsymbol{r}_2 e^{-z_2/2\mu l_e}\frac{e^{ik\hat{\boldsymbol{s}}_e.\boldsymbol{r}_2}}{4\pi R}e^{-z_1/2\mu l_e}\frac{e^{-ik\hat{\boldsymbol{s}}_e.\boldsymbol{r}_1}}{4\pi R}\Gamma(\boldsymbol{r}_1,\boldsymbol{r}_2)\\ &\times\ e^{-z_1/2l_e}e^{-z_2/2l_e}e^{-ik\hat{\boldsymbol{s}}_i.\boldsymbol{r}_1}e^{ik\hat{\boldsymbol{s}}_i.\boldsymbol{r}_2}\quad , \end{aligned} \quad (8.20)$$

so that

$$\boxed{\alpha_c(\hat{\boldsymbol{s}}_e) = \frac{1}{(4\pi)^2 S}\int d\boldsymbol{r}_1 d\boldsymbol{r}_2 e^{-\left(\frac{\mu+1}{2\mu}\right)\frac{z_1+z_2}{l_e}}\Gamma(\boldsymbol{r}_1,\boldsymbol{r}_2)e^{ik(\hat{\boldsymbol{s}}_i+\hat{\boldsymbol{s}}_e).(\boldsymbol{r}_2-\boldsymbol{r}_1)}} \quad (8.21)$$

The phase that appears in this relation leads to an angular dependence of the Cooperon contribution to the albedo. It is also important to notice that the exponential attenuation factors appearing in relations (8.10) and (8.21) are different. Along the *backscattering direction*, defined by the condition $\hat{\boldsymbol{s}}_i + \hat{\boldsymbol{s}}_e = 0$, the phase factor disappears and, since $\mu = 1$, we obtain

$$\alpha_c(\theta = 0) = \alpha_d \quad (8.22)$$

where θ is the angle between the incident and emergent directions $\hat{\boldsymbol{s}}_i$ and $\hat{\boldsymbol{s}}_e$, as represented in Figure 8.2. Therefore the total average albedo $\alpha(\theta) = \alpha_d + \alpha_c(\theta)$ is such that

$$\boxed{\alpha(\theta = 0) = 2\alpha_d} \quad (8.23)$$

This relation should be compared with the doubling of the probability to return to the origin due to the Cooperon contribution as discussed in section 4.6. The corresponding physical phenomenon is usually known as *coherent backscattering*.

Using the relation (4.63) between the structure factor Γ and P_d, (8.21) becomes

$$\alpha_c = \frac{c}{4\pi l_e^2}\int_0^\infty dz_1 dz_2\ e^{-\left(\frac{\mu+1}{2\mu}\right)\frac{z_1+z_2}{l_e}}\int_S d^2\boldsymbol{\rho}\, P_d(\boldsymbol{\rho},z_1,z_2)\ e^{i\boldsymbol{k}_\perp.\boldsymbol{\rho}}\quad , \quad (8.24)$$

where $\boldsymbol{k}_\perp = (\boldsymbol{k}_i + \boldsymbol{k}_e)_\perp = k(\hat{\boldsymbol{s}}_i + \hat{\boldsymbol{s}}_e)_\perp$ is the projection on the xOy plane of the vector $\boldsymbol{k}_i + \boldsymbol{k}_e$. If the length of $(\hat{\boldsymbol{s}}_i + \hat{\boldsymbol{s}}_e)$ is small enough, we can neglect its projection along the z-axis. Using both relation (8.14) and the integral

$$\int_S d^2\boldsymbol{\rho}\, \frac{e^{i\boldsymbol{k}_\perp \cdot \boldsymbol{\rho}}}{\sqrt{\rho^2 + A^2}} = 2\pi \frac{e^{-k_\perp |A|}}{k_\perp} \quad , \tag{8.25}$$

with the notation $k_\perp = |\boldsymbol{k}_\perp|$, we obtain

$$\boxed{\alpha_c = \frac{c}{4\pi l_e^2} \int_0^\infty dz_1 dz_2\; e^{-\left(\frac{\mu+1}{2\mu}\right)\frac{z_1+z_2}{l_e}} P_d(k_\perp, z_1, z_2)} \tag{8.26}$$

with [7]

$$P_d(k_\perp, z_1, z_2) = \frac{1}{2Dk_\perp} \left(e^{-k_\perp |z_1 - z_2|} - e^{-k_\perp (z_1 + z_2 + 2z_0)} \right) \quad . \tag{8.27}$$

Upon integrating, relation (8.26) becomes

$$\boxed{\alpha_c(k_\perp) = \frac{3}{8\pi} \frac{1}{\left(k_\perp l_e + \frac{\mu+1}{2\mu}\right)^2} \left(\frac{1 - e^{-2k_\perp z_0}}{k_\perp l_e} + \frac{2\mu}{\mu + 1} \right)} \tag{8.28}$$

As for the incoherent albedo, the dependence of $\alpha_c(\theta)$ on μ is negligible. In most calculations, we shall thus use the previous expression with $\mu = 1$, namely

$$\alpha_c(\theta) = \frac{3}{8\pi} \frac{1}{(1 + k_\perp l_e)^2} \left(1 + \frac{1 - e^{-2k_\perp z_0}}{k_\perp l_e} \right) \quad . \tag{8.29}$$

At small angles, we have $k_\perp \simeq \frac{2\pi}{\lambda}|\theta|$. The coherent contribution is non zero within a cone of angular aperture $\frac{\lambda}{2\pi l_e}$ near the backscattering direction ($k_\perp \to 0$). By expanding (8.29) we obtain

$$\alpha_c(\theta) \simeq \alpha_d \left(1 - 2\frac{(l_e + z_0)^2}{l_e + 2z_0} k_\perp \right) + O\left(k_\perp^2\right) \tag{8.30}$$

$$\simeq \alpha_c(0) - \frac{3}{4\pi} \frac{(l_e + z_0)^2}{l_e} k_\perp + O\left(k_\perp^2\right) \tag{8.31}$$

and $\alpha_c(0) = \alpha_d$. This result can be cast in the form

$$\alpha_c(\theta) \simeq \alpha_c(0) - \beta k_\perp l_e = \alpha_c(0) - \beta k l_e |\theta| \tag{8.32}$$

where the parameter β is defined by [211]

$$\beta = \frac{3}{4\pi} \left(1 + \frac{z_0}{l_e} \right)^2 = \frac{25}{12\pi} \tag{8.33}$$

[7] (8.27) can also be deduced from relation (5.157) and the correspondence (5.47).

with $z_0 = \frac{2}{3} l_e$. A *triangular singularity* thus appears in the angular dependence of the albedo. This singularity results from the diffusive character of the propagation of the light intensity and, in the next section, we show that it is a measure of the distribution of the lengths of the multiple scattering paths. At large angles, $\alpha_c \to 0$, and only the classical, incoherent, contribution of the Diffuson remains.

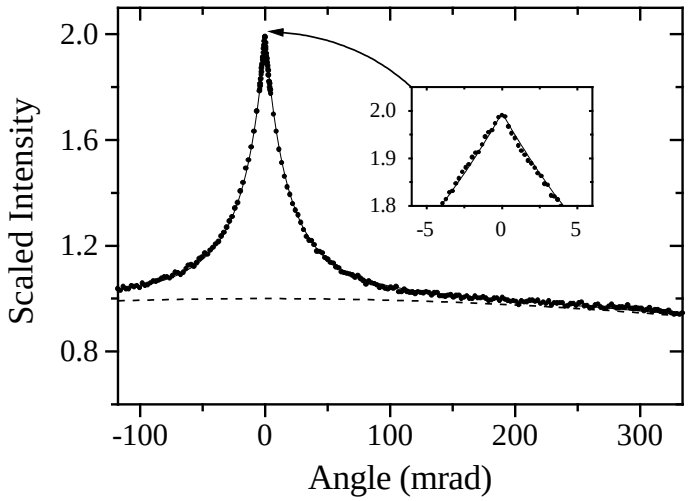

Figure 8.3: *Average intensity backscattered as a function of the angle θ, as measured in a powder (solid solution) of ZnO. The albedo at exact backscattering, i.e., for $\theta = 0$, is twice as large as its background value. In the inset, we see the triangular singularity. A more quantitative analysis of this behavior is given in section 8.8 [224].*

The expressions that we have just established for the coherent albedo were obtained using the diffusion approximation. We may question the validity of this approximation for the short multiple scattering trajectories. This point is discussed in section 8.8. An exact solution to the coherent albedo problem has been proposed for a scalar wave and isotropic scattering [216]. This solution is based on a slightly different formulation of the Milne problem (Appendix A5.3). The corresponding solution, obtained for a semi-infinite geometry, uses the Wiener-Hopf method and is inconvenient both for numerical handling and for comparing with experimental results. Moreover, it cannot be extended to more physical situations for which the scattering is anisotropic and the polarization of the waves plays a role. Nevertheless, it accounts for the contribution of the single scattering, an important point to which we shall return in section 8.8.2.

Exercise 8.1. Using relation (8.27), show that the expansion of $P_d(k_\perp, z_1, z_2)$ around $k_\perp \to 0$ is given by

$$P_d(k_\perp, z_1, z_2) = P_d(0, z_1, z_2) - \frac{k_\perp}{D}(z_1 + z_0)(z_2 + z_0) \quad . \tag{8.34}$$

Exercise 8.2. Modification of the albedo for a slab of finite width

How is the triangular singularity of the coherent backscattering peak modified when the diffusive medium is a slab of finite width L ? Show that in relation (8.30), $k_\perp$ must be replaced by $k_\perp \coth k_\perp(L + 2z_0)$.

For a finite width, we still keep the relation (8.26) and we replace (8.27) by (5.159), using the correspondence (5.47), namely

$$P_d(k_\perp, z_1, z_2) = \frac{1}{Dk_\perp} \frac{\sinh k_\perp(z_m + z_0) \sinh k_\perp(L + z_0 - z_M)}{\sinh k_\perp(L + 2z_0)} \tag{8.35}$$

with $z_m = min(z, z')$ and $z_M = max(z, z')$. We then expand this expression for small values of the arguments $k_\perp z_m$, $k_\perp z_M$ and $k_\perp z_0$, and we obtain a relation similar to (8.34) where $k_\perp$ has been replaced by $k_\perp \coth k_\perp(L+2z_0)$. Finally, the integral (8.26) leads to the announced result.
The aim of this exercise is to show that the characteristic cusp in the backscattering direction disappears for values of $k_\perp$ smaller than $1/L$. This singularity thus results from the contribution of long diffusive trajectories. Cutting off these trajectories beyond the length L modifies the cusp for small values of $k_\perp$, *i.e.*, for small angles. This relation between long trajectories and small angles is discussed in more detail in the next section.

More generally, using (8.35) and assuming $z_0 = 0$, show that for a slab of finite width L, the incoherent albedo $\alpha_d(L)$ and the coherent contribution $\alpha_c(k_\perp, L)$ are given by the expressions

$$\begin{aligned} \alpha_d(L) &= \frac{3}{8\pi}\left(1 - e^{-2b}\right)\left(1 - \frac{\tanh(b/2)}{b/2}\right) \qquad (8.36) \\ \alpha_c(k_\perp, L) &= \frac{3}{8\pi}\frac{1 - e^{-2b}}{(1 - k_\perp l_e)^2}\left[1 + \frac{2k_\perp l_e}{(1 + k_\perp l_e)^2}\frac{1 - \cosh\left(b\ \ (k_\perp l_e + 1)\right)}{\sinh b\ \ \sinh(b\ \ k_\perp l_e)}\right] \quad , \end{aligned}$$

valid only in the diffusive limit, *i.e.*, when the optical depth defined by $b = L/l_e$ becomes much larger than 1. Check that in the backscattering direction we still have the relation $\alpha_c(0, L) = \alpha_d(L)$, but without the cusp.

8.4 Time dependence of the albedo and study of the triangular cusp

Of interest is an alternative derivation of the albedo starting from the time dependence of the diffusion probability $P_d(\boldsymbol{r}, \boldsymbol{r}', t)$. For the geometry of a semi-infinite medium, with the help of relations (5.42) and (5.65), and the vanishing boundary condition at $-z_0$, we obtain

$$P_d(\boldsymbol{r}, \boldsymbol{r}', t) = \frac{e^{-\rho^2/4Dt}}{(4\pi Dt)^{3/2}}\left[e^{-(z-z')^2/4Dt} - e^{-(z+z'+2z_0)^2/4Dt}\right] \quad , \tag{8.37}$$

where we have taken for the two-dimensional Fourier transform, the expression $P_d(k_\perp, z, z', t)$,

$$P_d(k_\perp, z, z', t) = \frac{e^{-Dk_\perp^2 t}}{(4\pi Dt)^{1/2}} \left[e^{-(z-z')^2/4Dt} - e^{-(z+z'+2z_0)^2/4Dt} \right] \quad . \tag{8.38}$$

We can now define, at least formally, a time-dependent albedo $\alpha(t) = \alpha_d(t) + \alpha_c(\theta, t)$ by

$$\alpha_d = \int_0^\infty dt\ \alpha_d(t) \quad , \quad \alpha_c(\theta) = \int_0^\infty dt\ \alpha_c(\theta, t) \quad . \tag{8.39}$$

We consider the small angle limit so that $\mu = 1$ and the angular dependence of α_d is negligible. Noticing that $\alpha_c(0, t) = \alpha_d(t)$ and using (8.26), we obtain for $\alpha_d(t)$ and $\alpha_c(\theta, t)$ the two expressions

$$\alpha_d(t) = \frac{c}{4\pi l_e^2} \int_0^\infty dz dz'\ e^{-z/l_e} e^{-z'/l_e} P_d(z, z', t) \tag{8.40}$$

$$\alpha_c(\theta, t) = \frac{c}{4\pi l_e^2} \int_0^\infty dz dz'\ e^{-z/l_e} e^{-z'/l_e} P_d(k_\perp, z, z', t)\ . \tag{8.41}$$

The integrals over z and z' have no angular dependence. The only remaining angular dependence comes from the factor $e^{-Dk_\perp^2 t}$ that is nothing but the *Fourier transform of a two-dimensional diffusion process* restricted to the interface.

Because of the exponential factors that appear in the integrals over z and z', these integrals are cut off at a length of the order of the elastic mean free path l_e. Then, in the long time limit ($t \gg \tau_e$), the Gaussian terms in the brackets of (8.38) can be expanded. Upon integrating over z and z', we obtain

$$\alpha_c(\theta, t) = \alpha_d(t) e^{-Dk_\perp^2 t} \tag{8.42}$$

with

$$\alpha_d(t) \simeq c(z_0 + l_e)^2 \frac{1}{(4\pi Dt)^{3/2}} \tag{8.43}$$

and $k_\perp \simeq 2\pi|\theta|/\lambda = k|\theta|$. This expression allows to rewrite $\alpha_c(\theta, t)$ in the form

$$\alpha_c(\theta) \propto \int_0^\infty \frac{1}{t^{3/2}} e^{-\frac{1}{3}(kl_e\theta)^2 t/\tau_e} \left(1 - e^{-t/\tau_e}\right) dt \quad . \tag{8.44}$$

The integrand in this expression accounts for the contribution of diffusive trajectories of total length t. An additional factor $(1 - e^{-t/\tau_e})$ has been introduced in order to cut off the integral at small times.

In the backscattering direction ($k_\perp = 0$), we have $\alpha_c(\theta = 0, t) = \alpha_d(t) \propto (Dt)^{-3/2}$. At a given time t, the coherent backscattered echo is enhanced by a factor $(1 + e^{-Dk_\perp^2 t})$ as compared to its incoherent value. This enhancement occurs inside a cone whose angular aperture is $\theta(t) = \frac{\lambda}{2\pi\sqrt{Dt}}$, so that the

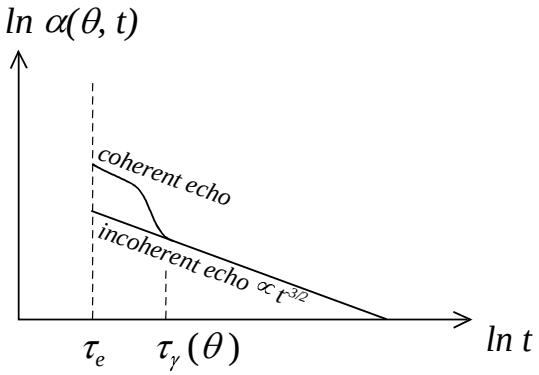

Figure 8.4: *Time dependence of the albedo $\alpha(\theta, t)$ at a fixed angle θ in a logarithmic plot. The coherent contribution appears for times shorter than $\tau_\gamma(\theta)$ given by the relation (8.47).*

smaller the length t of the diffusive paths, the larger is the angular aperture of their contribution to the coherent backscattering cone (Figure 8.4). This implies that in the backscattering direction, *the factor 2 between the coherent and incoherent contributions remains at all times.*

It is of interest that the albedo $\alpha_d(t)$ can be interpreted as the probability of reaching the plane $z = -z_0$ after a time t. This probability varies like $t^{-3/2}$ and does not depend on the space dimensionality, in the sense that the same result remains true for a two-dimensional diffusive process and a one-dimensional interface or more generally in d dimensions with a $(d-1)$-dimensional interface.

Another useful representation of the albedo $\alpha_c(\theta)$ is obtained in the form of the following Laplace transform

$$\alpha_c(\theta) = \int_0^\infty dt\ \alpha_d(t) \left\langle e^{i\boldsymbol{k}_\perp \cdot \boldsymbol{\rho}} \right\rangle \tag{8.45}$$

in which the average is taken using the Gaussian law :

$$\left\langle e^{i\boldsymbol{k}_\perp \cdot \boldsymbol{\rho}} \right\rangle = e^{-Dk_\perp^2 t} \quad . \tag{8.46}$$

The comparison of these two relations with (6.3) allows us to define a dephasing time $\tau_\gamma(\theta) = 1/Dk_\perp^2$, that can also be written as

$$\boxed{\frac{\tau_\gamma(\theta)}{\tau_e} = \frac{3}{(kl_e\theta)^2}} \tag{8.47}$$

The triangular cusp characteristic of the coherent backscattering can then be interpreted as arising from the sum of a series of Gaussian terms weighted by the probability $(Dt)^{-3/2}$. Although each of these terms behaves parabolically near backscattering $\theta \simeq 0$, the integral becomes singular around this value.

The angle θ thus appears as a variable conjugate to the length t of the diffusive paths. A given value of θ selects all paths of lengths $t/\tau_e \leq \frac{3}{(kl_e\theta)^2}$ that contribute to the coherent backscattering peak (Figure 8.4) . In other words, *long trajectories provide the main contribution to the coherent albedo at small angles*. The quantity $L_\gamma = \sqrt{D\tau_\gamma(\theta)} \simeq \lambda/2\pi\theta$ appears to be the characteristic length beyond which diffusive paths no longer contribute to the Cooperon and to the coherent backscattering cone. In that sense, L_γ can be viewed as a dephasing length (see Chapter 6) associated with the controlled and reversible phase shift driven by the angle θ.

8.5 Effect of absorption

The effect of absorption on the albedo can be accounted for by means of an *absorption length* l_a and the phenomenological expression [8]

$$\alpha(\theta, l_a) = \int_0^\infty dt\ \alpha(\theta, t)\ e^{-t/\tau_a} \tag{8.48}$$

where $\tau_a = l_a/c$ is the absorption time. Then, for the coherent albedo we obtain

$$\alpha_c(\theta, l_a) = \int_0^\infty dt\ \alpha_d(t) e^{-Dtk_\perp^2}\ e^{-t/\tau_a} \quad . \tag{8.49}$$

These expressions of coherent albedo in either the presence or the absence of absorption are related by

$$\boxed{\alpha_c(k_\perp, l_a) = \alpha_c\left(\sqrt{k_\perp^2 + k_a^2}, \infty\right)} \tag{8.50}$$

with $k_a^{-1} = \sqrt{D\tau_a} = \sqrt{\frac{l_e l_a}{3}}$. In the backscattering direction, the previous expression yields

$$\alpha_c(0, l_a) = \alpha_c(k_a, \infty) \quad . \tag{8.51}$$

The overall effect of a finite absorption length is to cut off the contributions of diffusive trajectories of length longer than $\sqrt{D\tau_a}$ both to the coherent and incoherent albedos. Based on the analysis presented in the previous section and on the expression (8.44), we expect the coherent albedo to exhibit a parabolic behavior for angles θ such that $\tau_\gamma > \tau_a$, or equivalently $\theta < \lambda/2\pi\sqrt{l_e l_a}$. This results from the suppression of the diffusive trajectories of length larger than $\sqrt{D\tau_a}$. Such a behavior has indeed been observed experimentally (see Figure 8.5 and section 8.8.3).

[8] Care must be taken to distinguish between the absorption length l_a defined as $l_a = c\tau_a$ which corresponds to a diffusive trajectory of total length τ_a, and the length $L_a = \sqrt{D\tau_a}$ which is the typical distance reached by diffusion in a time τ_a. The latter plays a role analogous to L_γ defined previously. It is usually more convenient to use l_a.

It is also of interest to compare the effect of a finite absorption length with that of a phase coherence time τ_ϕ as it appeared in the description of coherent transport in metals (section 7.4). Indeed it is important to notice that the absorption (τ_a) has a different effect than dephasing (τ_ϕ) since it affects both coherent and incoherent contributions, so that the factor 2 at backscattering remains unchanged. This is to be contrasted with the case of electrons where a finite τ_ϕ affects the coherent contribution responsible for weak localization by cutting off the trajectories of length longer than $\sqrt{D\tau_\phi}$ but leaves the incoherent contribution unchanged.

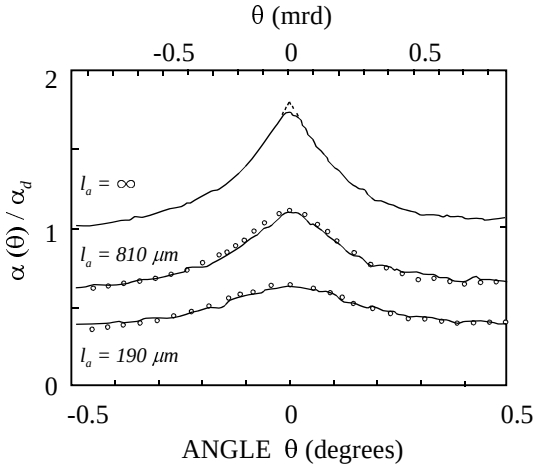

Figure 8.5: *Behavior of the albedo in the presence of absorption for different values of the absorption length l_a. See also Figure 8.11 [219].*

8.6 Coherent albedo and anisotropic collisions

So far, we have limited ourselves to the case of isotropic scattering. The only relevant characteristic length in the diffusive medium is then the elastic mean free path l_e. But in most physically relevant situations, the scattering is anisotropic and the transport mean free path l^* differs from the elastic mean free path l_e (Appendix A4.3). How is the albedo modified in that case? We still expect the diffusion approximation to describe the long multiple scattering trajectories properly, provided we replace D by D^* (*i.e.* l_e by l^*), so that the small angle behavior of the coherent albedo α_c remains unchanged. In other words, we expect (8.31) to still hold provided we replace l_e by l^* and z_0 by $\frac{2}{3}l^*$.

To understand better the distinct roles of l_e and l^*, let us start from the definitions (8.6) and (8.19) of the albedo. In the expression of α_d, the mean free path l_e appears in the average Green's functions and in the structure factor Γ. For the case of anisotropic scattering it seems justified to replace the diffusion coefficient D by D^* in the expression of Γ (relation 4.170). On the other hand,

the average Green's functions that account respectively for the first and last scattering events, remain functions of l_e and not of l^*. Performing the above mentioned changes leads straightforwardly to a set of expressions for the small angle coherent albedo and for the incoherent one, that depend on the ratio l_e/l^*, in contradiction to the argument presented in the first paragraph and, more importantly, to experimental results.

To grasp the nature of this apparent contradiction, it must be realized that the relations (8.6) and (8.19) need to be generalized in order to account for the angular dependence of the structure factor (relation 8.18). Instead, we now present an alternative description of light transport based on radiative transfer the details of which may be found in Appendix A5.2. Equation (5.93) for the specific intensity $I_d(\hat{\boldsymbol{s}}, \boldsymbol{r})$ relies on the same approximations as those for the Diffuson P_d. The advantage of the radiative transfer approach is that it allows a more systematic description that includes the geometry of the diffusive medium and the nature of the light sources. For instance, light sources appear explicitly in (5.93) and the nature of the boundaries sets the choice of the boundary conditions. Within the diffusion approximation used thus far for the calculation of the albedo, the radiative transfer equation reduces to the diffusion equation (5.105). But an advantage of the radiative transfer description as compared to (4.66) resides in the fact that it contains explicitly the source of the radiation. Another advantage is that it allows the conversion of an incident plane wave into a diffusing wave to be described simply with the boundary condition (5.108) of a vanishing incoming diffuse flux. In the absence of sources, this boundary condition is given by (5.113), and it depends on the extrapolation length $z_0 = \frac{2}{3}l^*$ we have been using previously. If there is a source, this boundary condition takes the form (5.129), which depends both on l^* and l_e.

The calculation of the albedo based on the radiative transfer equation and on this boundary condition is more consistent, although less intuitive, than the one that led to relations (8.16) and (8.28). But it is important to emphasize that these two descriptions rely on the diffusion approximation and, as such, they are equivalent. They differ in the fact that they do not treat the contribution of the short multiple scattering trajectories on the same footing.

To proceed further, we again consider the geometry of a semi-infinite diffusive medium whose interface is illuminated by a point-like light source of intensity $I_0\delta(\boldsymbol{\rho})$, in which $\boldsymbol{\rho}$ is a vector contained in the plane $z = 0$ defining the interface. We have shown that the average intensity $I_d(\boldsymbol{r})$ is, at the diffusion approximation, the solution of the equation (5.105) with the boundary condition (5.129). For the geometry of a slab, the solution of this problem is given by (5.132), namely

$$I_d(\boldsymbol{\rho}, z = 0) = \frac{I_0}{4\pi^2}\frac{l^*}{l_e}\int_0^\infty d\lambda\ J_0(\lambda\rho)\ \frac{\lambda}{1 + \frac{2}{3}l^*\lambda}\ \left(\frac{1}{1 + \lambda l_e} - \eta\right) \qquad (8.52)$$

where $\eta = 1 - l_e/l^*$ and J_0 is a Bessel function. The outgoing flux at a point of the interface is given by (5.131), namely $\frac{5}{2}I_d(\boldsymbol{\rho}, z = 0)$ [217, 210]. The coherent albedo is simply given by the Fourier transform of this flux with respect to the

variable $\boldsymbol{\rho}$:

$$\alpha_c(\theta) = \frac{5}{2I_0} \int_S d^2\boldsymbol{\rho}\, I_d(\boldsymbol{\rho}, z=0)\; e^{i\boldsymbol{k}_\perp \cdot \boldsymbol{\rho}} \quad . \tag{8.53}$$

The integral over $\boldsymbol{\rho}$ is easily performed using (15.61). We obtain finally

$$\boxed{\alpha_c(\theta) = \frac{5}{4\pi} \frac{1}{1-\eta}\; \frac{1}{1+\frac{2}{3}k_\perp l^*}\; \left(\frac{1}{1+k_\perp l_e} - \eta\right)} \tag{8.54}$$

In the small angle limit, only long diffusive trajectories contribute to α_c, which then happens to depend only on the transport mean free path l^*, as stated previously. In this limit, the expression (8.54) rewrites

$$\alpha_c(\theta) \simeq \alpha_d - \beta^* k_\perp l^* = \alpha_d - \beta^* k l^* |\theta| \tag{8.55}$$

with

$$\beta^* = \frac{3}{4\pi} \left(1 + \frac{z_0}{l^*}\right)^2 \quad . \tag{8.56}$$

By inserting $z_0 = 2l^*/3$, we notice that $\beta^* = 25/12\pi$, *i.e.*, that it is independent of the exact nature of the scattering process [9] (see 8.33). The expression (8.54) for α_c does not apply in the large angle limit (it gives an overall negative value to the total albedo) since its range of validity is restricted to the diffusion approximation, *i.e.*, to diffusive trajectories of length longer than l^*.

8.7 The effect of polarization

Up to now, we have considered the Cooperon contribution to the coherent albedo under the assumption that the light is a scalar wave, thus ignoring the effect of polarization. We now reconsider this assumption. We saw in section 6.6 that the effect of polarization is to introduce a phase shift between paired sequences of multiple scattering. Here we discuss this phase shift in the framework of the Rayleigh approximation [10] (sections A2.1.4 and 6.6). We shall consider a linearly polarized (denoted by l) or a circularly polarized wave characterized by its helicity h.

[9] To the best of our knowledge, there is no full fledged "microscopic" calculation of the albedo for the case of anisotropic scattering. Moreover, it would not be very useful since such an expression of the albedo at large angles would necessarily depend on other parameters so far neglected (*e.g.* polarization, optical index mismatch, etc.). Nevertheless, it is worth mentioning the result obtained in reference [218] for the coherent albedo in the anisotropic case, that was obtained by combining together a microscopic description and the radiative transfer approach. The absolute slope obtained by these authors is $-3/4\pi(z_0/l^* + l_e/l^*)^2$. It depends on l_e whereas it is expected to be universal.

[10] The results obtained in this approximation can be readily extended to the case of Rayleigh-Gans scattering (remark p. 253).

8.7.1 Depolarization coefficients

In section 6.6 we have studied the evolution of a given polarization state of a light beam under multiple scattering. This evolution is described by the integral equation (6.156). A first and obvious effect of multiple scattering is the depolarization of the incident light. After a time t (*i.e.*, for diffusive trajectories of length ct), the depolarization of a wave can be characterized with the help of two depolarization coefficients $d_{\parallel}(t)$ and $d_{\perp}(t)$ which measure the relative intensity analyzed in the backscattering direction, within each polarization channel respectively parallel ($l \parallel l$ or $h \parallel h$) and perpendicular ($l \perp l$ or $h \perp h$) to the incident polarization. These coefficients are defined by

$$d_{\parallel}(t) = \frac{\Gamma_{\parallel}^{(d)}(t)}{\Gamma_{\parallel}^{(d)}(t) + \Gamma_{\perp}^{(d)}(t)} \quad , \quad d_{\perp}(t) = \frac{\Gamma_{\perp}^{(d)}(t)}{\Gamma_{\parallel}^{(d)}(t) + \Gamma_{\perp}^{(d)}(t)} \quad , \tag{8.57}$$

where $\Gamma_{\parallel}^{(d)}$ and $\Gamma_{\perp}^{(d)}$ are the amplitudes of the structure factor in the corresponding polarization channels. Clearly, in the long time limit, the depolarization is complete :

$$d_{\parallel}(t) \underset{t\to\infty}{\longrightarrow} \frac{1}{2} \quad , \quad d_{\perp}(t) \underset{t\to\infty}{\longrightarrow} \frac{1}{2} \; . \tag{8.58}$$

This results from the fact that the contribution of the scalar mode Γ_0 is not attenuated and is the same in the different components $\Gamma_{\alpha\alpha,\beta\beta}$ of the structure factor (see eqs. 6.173, 6.174), so that the contribution of long trajectories ($t \to \infty$) to the intensity is the same in all polarization channels.

Depolarization affects equally the coherent and incoherent contributions to the albedo, *i.e.*, the Diffuson and the Cooperon. This effect must be taken into account to describe properly the multiple scattering of an initially polarized light. For instance, the incoherent albedo is obtained from expression (8.39), which after inserting the time dependent depolarization factors, becomes

$$\alpha_d^{\parallel} = \int_0^{\infty} dt\, \alpha_d(t) d_{\parallel}(t) \simeq \frac{1}{2}\alpha_d \tag{8.59}$$

$$\alpha_d^{\perp} = \int_0^{\infty} dt\, \alpha_d(t) d_{\perp}(t) \simeq \frac{1}{2}\alpha_d \quad . \tag{8.60}$$

The net effect of depolarization is to reduce the incoherent background described by $\alpha_d^{\perp}$ and $\alpha_d^{\parallel}$ almost in the same proportion. Half of the signal is detected in each of the two polarization channels, parallel and perpendicular. The approximation $d_{\parallel,\perp} \simeq \frac{1}{2}$ is well justified for the almost fully depolarized long trajectories, that is for times larger than the characteristic times τ_1 and τ_2 of the decaying modes (eq. 6.166). On the other hand, the weight of short trajectories, still partially polarized, is then underestimated.

8.7.2 Coherent albedo of a polarized wave

In addition to depolarization, there is an additional phase shift between multiple scattering sequences propagating in opposite directions. This phase shift

thus affects the Cooperon and the coherent backscattering. To see how this happens, we consider an incident polarized beam. The coherent albedo can be analyzed either in the same polarization channel or in the perpendicular one. We have shown in section 6.6.4 that if the light is analyzed in the same polarization channel, the vectorial nature of the light does not play any role, apart from the depolarization effects previously discussed. The corresponding coherent albedo $\alpha_c^{\parallel}$, obtained from (8.44), remains unchanged and it includes only the depolarization (8.58) of the incident light :

$$\alpha_c^{\parallel}(\theta) = \int_0^{\infty} \alpha_d(t) d_{\parallel}(t) e^{-Dt\left(\frac{2\pi}{\lambda}\theta\right)^2} (1 - e^{-t/\tau_e}) dt \quad . \tag{8.61}$$

Is this result also true for the perpendicular channel? For an initially polarized light, the coherent albedo analyzed in the perpendicular channel is attenuated by a multiplicative factor $Q_{\perp}(t)$ defined as the ratio of the Cooperon and the Diffuson contributions to the structure factor :

$$Q_{\perp}(t) = \frac{\Gamma_{\perp}^{(c)}(t)}{\Gamma_{\perp}^{(d)}(t)} \quad . \tag{8.62}$$

This ratio vanishes at large times, since the Cooperon in the perpendicular channel involves two rapidly decaying modes $k = 1$ and $k = 2$ (see eqs. 6.176 and 6.167), whereas $\Gamma_{\perp}^{(d)}(t)$ is driven by the Goldstone mode Γ_0, see the discussion p. 251. The coherent albedo $\alpha_c^{\perp}(\theta)$ becomes

$$\alpha_c^{\perp}(\theta) = \int_0^{\infty} \alpha_d(t) d_{\perp}(t) Q_{\perp}(t) e^{-Dt\left(\frac{2\pi}{\lambda}\theta\right)^2} (1 - e^{-t/\tau_e}) dt \,. \tag{8.63}$$

For a beam analyzed along a polarization parallel to the incident one, we check using (8.59) and (8.61) that $\alpha_c^{\parallel}(\theta = 0) = \alpha_d^{\parallel}$. Therefore, as a result of depolarization, both coherent and incoherent contributions are reduced by half, but their ratio remains unchanged, namely there is still a factor 2 for the coherent backscattering peak as in the scalar case. On the other hand, for an emergent beam analyzed in a channel perpendicular to the incident one, the coherent albedo becomes reduced due to the exponential decay of the Cooperon $\Gamma_{\perp}^{(c)}(t)$ at large time. Consequently, the contribution of long diffusive trajectories is reduced. The ratio between the coherent and incoherent contributions in backscattering ($\theta = 0$) is thus given by

$$r = \frac{\int_0^{\infty} dt\, \alpha_d(t) d_{\perp}(t) Q_{\perp}(t)}{\int_0^{\infty} dt\, \alpha_d(t) d_{\perp}(t)} \quad . \tag{8.64}$$

The height of the cone is then reduced. The behaviors described above have been observed experimentally, and are represented in Figure 8.6. We should keep in mind that the previous results apply only for the limiting case of Rayleigh scattering. For bigger scatterers, which is the common case, we deal with anisotropic Mie scattering. The depolarization thus occurs on longer multiple scattering trajectories.

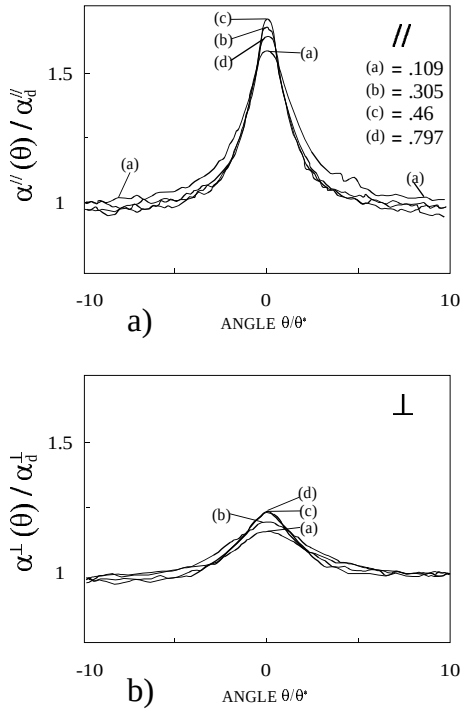

Figure 8.6: *Angular behavior of the coherent backscattering peak for a linearly polarized light which is analyzed a) along the same polarization channel, and b) along the perpendicular channel. The diffusive medium is made of polystyrene spheres of diameters* $0.109\mu m$, $0.305\mu m$, $0.460\mu m$ *and* $0.797\mu m$. *The angles are scaled by the peak widths* (θ^*) *and the intensities by the multiply scattered* ($\|$) *incoherent intensity so that all curves have the same width [219].*

8.8 Experimental results

In the introduction of this chapter, we gave a brief historical overview of the study of coherent backscattering. In the first measurement of an interference effect near the backscattering direction [206], the relative enhancement factor was about 15% instead of the expected 100% predicted theoretically. This partly explains why this effect was not observed beforehand, even by chance. The angular aperture of the cone, given by the ratio λ/l^*, is of the order of a few *mrad* only. Its observation thus requires a very sensitive angular resolution which has been achieved only quite recently. Following this first observation and triggered by a number of theoretical predictions, several groups have designed more and more precise experimental setups. The existing experiments can be divided into two main groups : those performed on diffusive media made of liquid suspensions of scatterers [206, 207, 208, 219] and those using solid solutions [221, 222, 223]. In the first setting, the average results simply from the motion of the scatterers integrated over a long enough time. In the second

case, the average is obtained either by collecting the results obtained from different configurations or by rotating a cylindrical sample along its axis, each position providing a different configuration. The equivalence of the results obtained from these different methods can be viewed as a justification of the ergodic hypothesis.

The best angular resolution obtained so far is less than $50\mu rad$ [223]. A good angular resolution is an experimental constraint for the observation of the effects predicted theoretically, namely the factor 2 enhancement of the coherent albedo and the triangular cusp near the backscattering direction. The experimental confirmation of these predictions has paved the road to the quantitative study of the other effects presented in this chapter, *i.e.*, those related to the presence of absorption, the size of the scatterers, the role of polarization, etc. The results that have been obtained demonstrate beyond any doubt that, besides the good understanding of coherent backscattering, we now have at our disposal a tool that allows us to characterize very precisely multiple scattering systems.

8.8.1 The triangular cusp

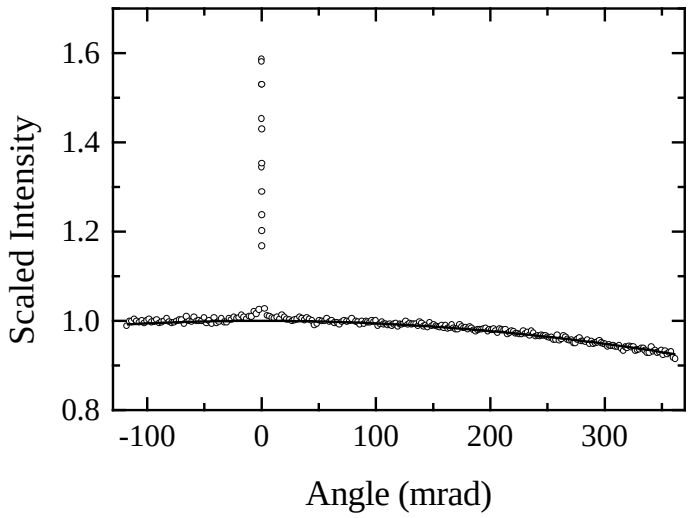

Figure 8.7: *Angular dependence of the intensity backscattered by a sample of teflon. The extremely narrow cone results from the large elastic mean free path. The intensity is normalized to one near zero angle. The continuous line corresponds to a fit using the expression (8.16) for* α_d *[224].*

In the course of our study of coherent albedo, we have assumed that the incoherent albedo α_d has no angular structure. This appears clearly in Figure 8.7 which presents the backscattering by teflon. In Figure 8.8, we observe the enhancement by a factor 2 and the cusp characteristics of coherent backscattering. The agreement between these experimental results and expression (8.28)

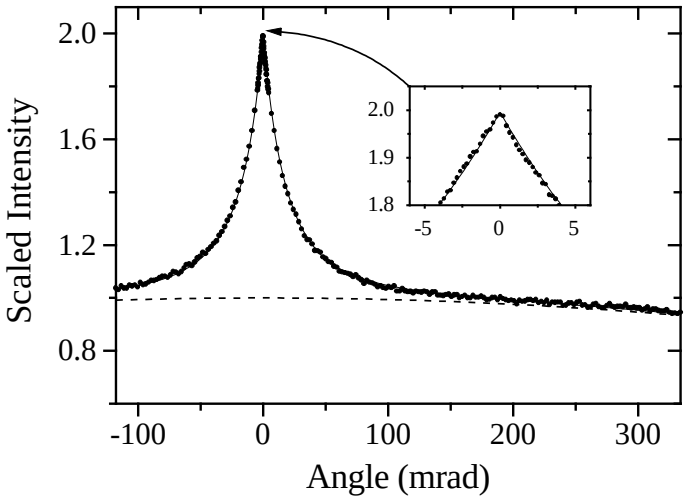

Figure 8.8: *Angular dependence of the intensity backscattered by a powder (solid solution) of ZnO. The elastic mean free path is* $l^* = 1.9 \pm 0.1 \mu m$*. The normalization is such that the incoherent contribution (dashed line) is equal to one in the backscattering direction* ($\theta = 0$)*. The enhancement factor is* $\alpha(\theta = 0) = 1.994 \pm 0.012$*. The continuous line corresponds to the expression (8.28) established in the diffusion approximation (weighted by a factor* $1/2$ *that accounts for depolarization). The inset shows the behavior of the coherent albedo near backscattering and the triangular cusp fitted using expression (8.28) [224].*

is excellent, both for liquid and solid solutions, and for a broad range of wavelengths and of elastic mean free paths [223, 224]. This agreement nevertheless raises a number of questions, bearing in mind the approximations underlying the derivation of expression (8.28). It has indeed been obtained for a scalar wave and within the diffusion approximation which is well justified only for long trajectories, *i.e.*, for small angles. This approximation underestimates the relative weight of short trajectories as compared to the exact solution [216].

This excellent agreement can be partially explained by the role played by polarization. We have indeed obtained that, for a polarized wave analyzed along the incident polarization channel, there is no phase shift between the two trajectories paired into the Cooperon, thus justifying the use of a scalar wave. Moreover, in contrast to long trajectories, the short ones are only partially depolarized, as shown by relations (8.58). As a result of their remaining polarization, the contribution of these short trajectories is partially washed out when it is analyzed along the incident polarization channel [11]. The contribution of the short trajectories is not, then, as important as predicted by the exact scalar theory.

[11] The same argument applies equally to the justification for neglecting the single scattering contribution to α_c, since it remains fully polarized.

8.8.2 Decrease of the height of the cone

Figure 8.9 shows that the width of the coherent backscattering cone decreases when l^* increases as predicted by (8.55). We also notice in the inset of the same figure that the height also depends on the mean free path. It decreases with l^* and reaches values smaller than the expected factor 2.

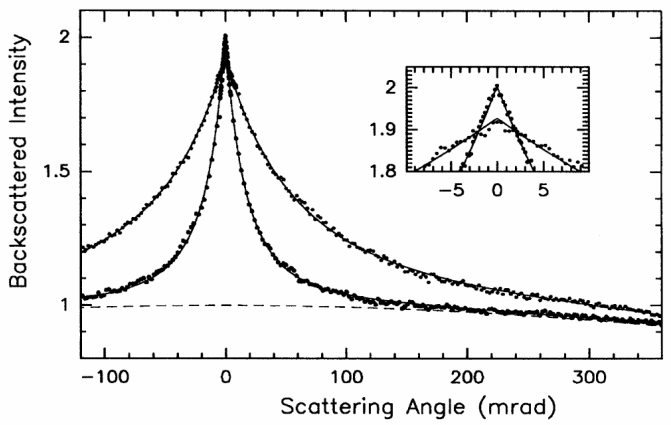

Figure 8.9: *Two measurements of the coherent backscattering cone that correspond respectively to a small value of l^* (broad cone) and to a larger value (narrow cone). The latter corresponds to a solid solution ($BaSO_4$) characterized by the parameter $kl^* = 22.6 \pm 1.0$, whereas the broader cone corresponds to a liquid suspension of TiO_2 characterized by $kl^* = 5.8 \pm 1.0$. The solid and dashed line curves correspond respectively to the relations (8.28) and (8.16). In the inset, we see clearly the deviation from factor 2 for the smallest value of l^* [223].*

A first and immediate source for this discrepancy is single scattering. Let us recall that in our respective calculations of the Diffuson and the Cooperon, we have included in the latter the single scattering contribution for the sake of convenience only (footnote 13, p. 123). However, it does not contribute to the coherent albedo since it is angle-independent, whereas it does contribute to the incoherent part α_d. Strictly speaking, to evaluate the enhancement factor $\mathcal{A}$, *i.e.*, the total value of the albedo at $\theta = 0$, we must take out of α_c the single scattering contribution α_0. With the help of the equality $\alpha_c = \alpha_d$, we thus obtain the relation

$$\mathcal{A} = \frac{(\alpha_c - \alpha_0) + \alpha_d}{\alpha_d} = 2 - \frac{\alpha_0}{\alpha_d} \quad . \tag{8.65}$$

As stated previously, polarization plays an important role in the behavior of the single scattering contribution to $\mathcal{A}$. For the case of Rayleigh scattering by point-like scatterers, single scattering is described by the differential scattering cross section (2.149) where the unit vectors $\hat{\boldsymbol{\varepsilon}}_i$ and $\hat{\boldsymbol{\varepsilon}}'$ account for the polarization of the incident and emergent fields, respectively. Those vectors define four

possible polarization channels : for a linearly polarized incident wave, we have two channels ($l \parallel l$) or ($l \perp l$), while for a circularly polarized incident wave, we have the two other channels ($h \parallel h$) and ($h \perp h$) where h is the helicity defined with respect to the direction of propagation.

For the case of single scattering, $\hat{\varepsilon}_i \cdot \hat{\varepsilon}'^*$ remains finite in backscattering only when ($l \parallel l$) or ($h \perp h$) (see Exercise 2.4). The latter channel describes a reflection in a mirror of a circularly polarized wave. It is thus possible, using channels ($l \perp l$) or ($h \parallel h$), to get rid of the single scattering contribution in backscattering for the Rayleigh case. Moreover, relation (8.63) indicates that in the channel ($l \perp l$) there is a non zero phase shift between the multiple scattering trajectories paired into the Cooperon. This is not the case of the channel ($h \parallel h$) for which the attenuation factor $\langle Q_{\alpha\alpha} \rangle = \langle Q_{\parallel} \rangle = 1$ (relation 8.62) [226]. It is thus possible, in this channel ($h \parallel h$), to obtain an enhancement factor equal to its maximum 2, since both the single scattering and the finite phase shift in the Cooperon are absent.

For anisotropic scattering, *i.e.*, in the Mie regime (section A2.3.2), all polarization channels contribute to backscattering. This leads to a smaller enhancement factor. In most cases, however, the anisotropy of the scattering cross section makes the single scattering contribution negligible in backscattering, thus restoring an enhancement factor close to 2.

Yet another contribution to a reduction of $\mathcal{A}$ exists. It originates in multiple scattering processes in which the wave is scattered more than once by a given scatterer. This contribution is independent of the angle θ, and therefore is added to the incoherent background, thus reducing $\mathcal{A}$. It has been calculated for the case of two scattering events [223] and it modifies the α_0 term in $\mathcal{A}$ by a factor proportional to $1/kl^*$. This behavior is in good agreement with the results shown in Figure 8.10.

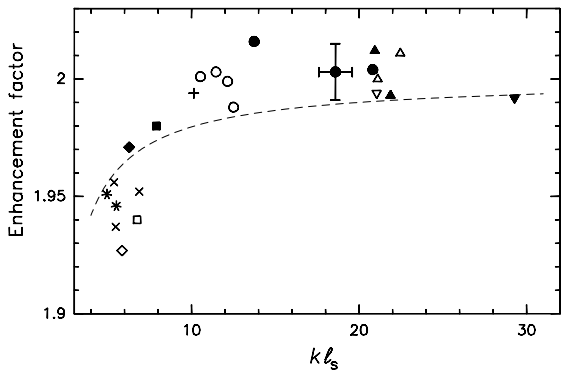

Figure 8.10: *Deviation of the amplification factor $\mathcal{A}$ with respect to the value $\mathcal{A} = 2$ plotted as a function of the parameter kl^*. Each point corresponds to a different solid solution. The dashed line results from a calculation of $\mathcal{A}$ which incorporates double scattering on the same scatterer [223].*

8.8.3 The role of absorption

The role of absorption in coherent backscattering does not simply amount to a decrease in the height of the cone as given by (8.50). The introduction of a new characteristic length l_a allows a more quantitative study of the comparative roles of l^* and l_e for the case of anisotropic scattering [219].

For instance, the results given in Figure 8.11 were obtained for a liquid suspension of polystyrene spheres of diameter $0.46\mu m$ and a light of wavelength $\lambda = 0.389\mu m$, a situation that corresponds to a very anisotropic scattering [12]. The absorption length l_a measured independently at this concentration of scatterers is of the order of $100\mu m$. From (8.48), we expect to suppress the contributions of the long trajectories. This is indeed what is observed in the parallel polarization channel [219, 225]. From a closer inspection of Figure 8.11, we also notice the following points relative to the effect of absorption :

- The incoherent contribution to the albedo is equally reduced in each of the two polarization channels, either parallel or perpendicular. This indicates that the contribution of the long trajectories to the incoherent albedo is fully depolarized.
- The height of the coherent albedo peak measured in the parallel polarization channel decreases in the same way as the incoherent background. This is in contrast to the case of the perpendicular polarization channel where the coherent albedo appeared to be much less affected. From this observation, we conclude that, without absorption, all the trajectories contribute to α_c in the parallel channel, whereas only a fraction of those trajectories do contribute in the perpendicular channel. This observation is in agreement with the conclusions of section 8.7.

Let us now proceed along the same line of thought but in a more quantitative way. The two expressions (8.50) and (8.51) provide a relation between the coherent albedo curves in the presence and in the absence of absorption, but at different angles. For instance, relation (8.51)

$$\alpha_c(0, l_a) = \alpha_c(k_a, \infty) \tag{8.66}$$

allows us to define for each value of l_a an angle $\theta_a = \lambda k_a / 2\pi$, such that

$$\theta_a = \frac{\lambda}{2\pi}\sqrt{\frac{3}{l_a l^*}} \quad . \tag{8.67}$$

Figure 8.12 shows this dependence of θ_a as a function of l_a. From this relation it is possible to deduce an experimental value for the transport mean free path, $l^* = 20 \pm 2\mu m$ which is pretty close to the calculated value ($21.5\mu m$) (see footnote 12, p. 367). The validity of the scaling behavior (8.50) which appears clearly in Figure 8.11 justifies once again the use of the diffusion approximation.

[12] The calculation of l^* using Mie scattering theory for spheres with this diameter yields $l^* = 21.5\mu m$, whereas $l_e = 4.1\mu m$ (section A2.3.2).

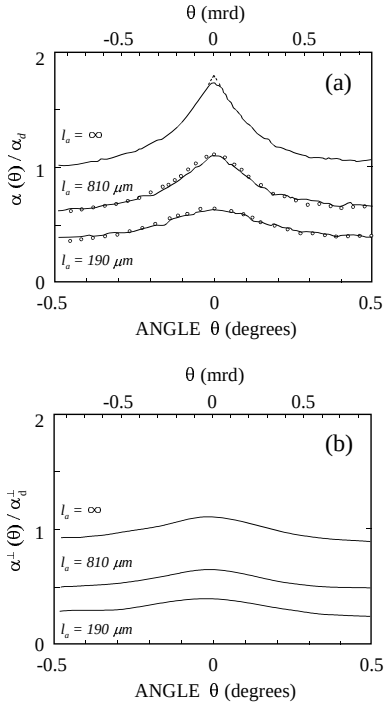

Figure 8.11: *Effect of the absorption on the behavior of the albedo in a medium made of a suspension of polystyrene beads immersed in a dye solution. Fig. (a) shows the coherent albedo in the polarization channel parallel to the incident polarization. The points are obtained using the scaling relation (8.50) which relates the coherent albedo in the presence and in the absence of absorption. (b) Same as in (a) but in the perpendicular polarization channel [219].*

From this quantitative agreement, it is possible to infer a value of the parameter β^* given by (8.56). This is an important issue since it allows us to check the predictions presented in section 8.6 concerning the validity of the radiative transfer approach. Within the parallel polarization channel, the coherent and incoherent contributions to the albedo are equally affected by absorption. In this channel, we thus have for the respective behavior of these two quantities, the relation

$$\alpha_d(l_a = \infty) - \alpha_d(l_a) = \alpha_c(k_a = 0) - \alpha_c(k_a) \tag{8.68}$$

which, once we expand $\alpha_c(k_a)$ for small values of k_a using (8.55), gives

$$\alpha_d(l_a) - \alpha_d(\infty) = -\frac{1}{2}\beta^* l^* k_a \quad , \tag{8.69}$$

where the factor $1/2$ has been added to account for depolarization effects. The use of this expression is well justified since it describes only the contribution of the long trajectories, (*i.e.*, the limit of small angles). Using $z_0/l^* = 2/3$, we infer from (8.56) the theoretical value $\beta^*/2 = 4.16/4\pi$. From an independent

measurement of $\alpha_d(\infty)$ in the absence of absorption and for point-like scatterers [219], we obtain an experimental value $\beta^*/2 = 4.2/4\pi \pm 20\%$ very close to the theoretical value. This is an important result : first it confirms that we cannot fix $z_0 = 0$ for the extrapolation length that enters into the calculation of the albedo of a semi-infinite medium, and, moreover, it also justifies using the value $z_0 = 2l^*/3$ obtained within the diffusion approximation. Second, it confirms the assumptions given in section 8.6 which led us to the conclusion that the slope of the albedo at small angles depends solely on l^* and not on l_e [13].

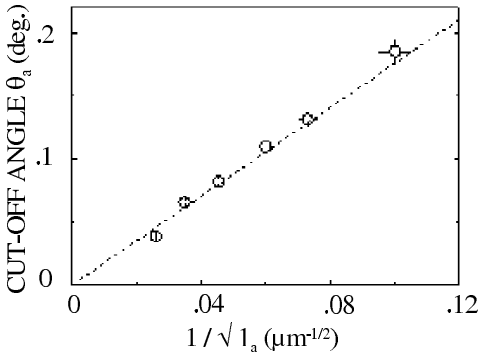

Figure 8.12: *Plot of the behavior of the angle θ_a defined by (8.67) as a function of the absorption length. The dashed line corresponds to (8.67) [219].*

8.9 Coherent backscattering at large

The interference effect underlying coherent backscattering is shared by many different physical systems and can be observed using a large variety of waves. The very existence of the coherent backscattering effect, the relative ease of measuring it, and the good quantitative understanding we have of it, at least for small angles, has turned it into a tool used relatively frequently in order to display coherent multiple scattering and to obtain *in situ* precise measurements of the transport mean free path. Moreover, coherent backscattering is a robust effect, which, using light sources, can be measured on a broad range of materials (see Figure 8.13).

The coherent backscattering effect can also be observed using a non coherent light source such as sunlight. To obtain its expression in this limit, we must perform the convolution of the monochromatic coherent albedo with the spec-

[13] This result is to be compared with the result obtained in reference [218] which predicts for β^* the expression

$$\beta^* = -3/4\pi(2/3 + l_e/l^*)^2 \quad . \tag{8.70}$$

We would then obtain a much smaller value for β^* because of the large factor $l^*/l_e \simeq 5$ for the case of beads of diameter $0.46\mu m$.

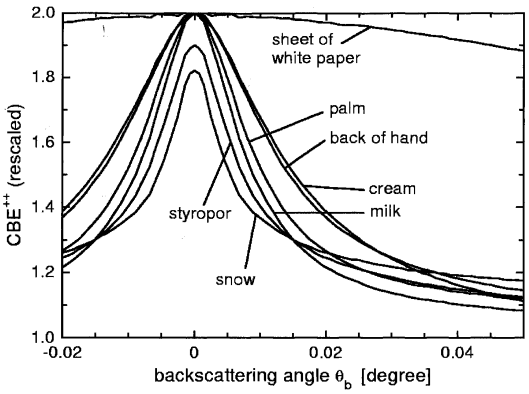

Figure 8.13: *Coherent backscattering cones measured using circularly polarized light of wavelength $\lambda = 0.514\mu m$ in various materials. The scales have been chosen so as to obtain an enhancement factor of 2 (apart from snow and styropor, for which the true angular variation has been plotted). The enhancement factors actually measured range between 1.6 and 2 [228].*

tral correlation function of the light source [227, 228]. For the case of sunlight, this yields to a reduction of the height of the cone (Figure 8.14).

8.9.1 Coherent backscattering and the "glory" effect

Other kinds of coherent backscattering effects have been observed for quite a long time. Among them, the most famous is perhaps the *glory* which shows up as a bright halo surrounding the shadow of a plane (or of a mountain hiker) projected onto a sea of clouds (Figure 8.15) [229]. In contrast to the coherent backscattering effect, the glory is a single scattering interference effect.

It results from the interference between equally long light paths inside a spherical drop of water [14] (Figure 8.16). The counting of all paths that contribute to the glory effect constitutes a difficult problem which necessitates the use of the Mie theory (section A2.3.2), and which depends on many parameters such as the wavelength of the incident light, the radius of the drop, and its optical index. The increase in the backscattered intensity occurs inside a cone of aperture of the order of λ/a, where a is the radius of the drop. For water inside clouds, this radius is about a few tens of microns, *i.e.*, much smaller than the transport mean free path of light in this medium. This explains why the bright halo that is observed is essentially associated with glory effect and not with coherent backscattering. For big enough scatterers, however, the two effects may coexist, and it could then be possible to cross over continuously from a regime where multiple scattering mainly occurs inside a scatterer to a regime of multiple scattering between scatterers [230].

[14] It might be of interest to note at this point that glory is an effect very different from the rainbow, which apart from supernumerary rainbows inside the main arc, is not an interference effect.

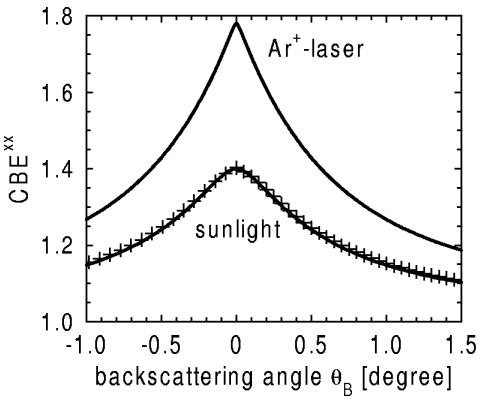

Figure 8.14: *Coherent backscattering cone obtained for sunlight on a solid solution of $BaSO_4$ and compared, for the same medium, to a monochromatic light of wavelength $\lambda = 0.514\mu m$ [228].*

Figure 8.15: *Glory observed along the Hörnli ridge on mount Cervin (picture G. Montambaux).*

8.9.2 Coherent backscattering and opposition effect in astrophysics

As early as 1887, it was observed that the sunlight intensity reflected by the rings of Saturn was larger in the backscattering direction [231] [15]. This observation was then extended to almost all the planets and their moons when observed in the so-called opposition configuration, *i.e.* when the Sun, Earth and planet of interest are aligned, thus giving to this increase of the backscattered intensity (Figure 8.17) the name "opposition effect." Various explanations for this effect have been proposed [232], but it is only recently that an explanation based on the coherent backscattering effect has been suggested [233].

It has also been observed that the difference $d_{\parallel} - d_{\perp}$ between the depolarization coefficients defined in (8.58) vanishes in the backscattering direction

[15] In astronomy, the backscattering angle is often called the phase angle.

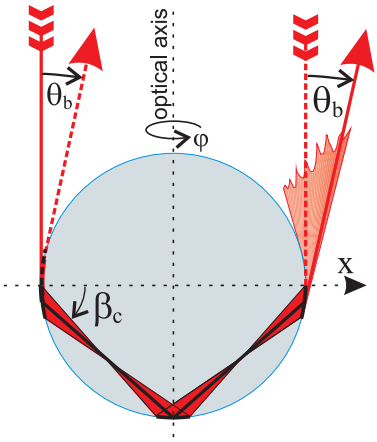

Figure 8.16: *Illustration of the typical optical paths that interfere to produce the glory effect. θ_b is the backscattering angle and β_c is the critical angle of total reflection [230].*

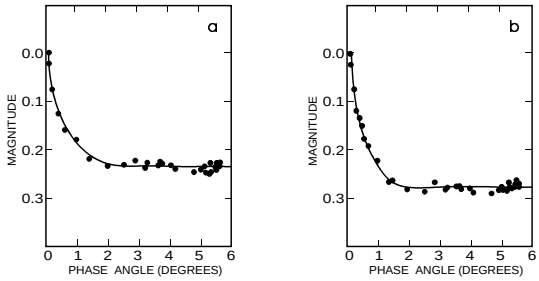

Figure 8.17: *Opposition effect observed on the rings A and B of Saturn with natural sunlight (a) and for blue light (b) (Franklin and Cook 1965).*

and becomes negative inside a cone of angular aperture roughly equal to that of the intensity [16]. This effect known as the "polarization opposition effect" was first observed by Lyot in 1929 [234]. It has been recently reexamined in great detail in the framework of polarization effects in multiple scattering. Those studies go much beyond the range of validity of the results presented in section 8.7. Actually, the scatterers (for instance small ice crystals) are much larger than the wavelength (Mie regime, section A2.3.2) and of random shape, so that the behavior of the polarization can only be obtained from numerical studies [226, 235]. The interpretation of the opposition effect in terms of coherent backscattering has indeed been fruitful, since it has led to a better understanding of the nature and composition of the measured reflecting surfaces. Nevertheless, we must still use this interpretation cautiously since a number of

[16] The definition (8.58) of the depolarization coefficients is general, but their expression has been obtained in the particular case of Rayleigh scattering.

questions remain unsolved. For instance, the angular aperture of the backscattering cone seems to correspond in certain cases to very short transport mean free paths l^*, a result at odds with the nature of the scatterers.

8.9.3 Coherent backscattering by cold atomic gases

The physics of cold atoms constitutes a very active field of research, especially since the first experimental observation in 1995 of the Bose-Einstein condensation in Rubidium atoms. The atomic densities reached in traps are very high, especially near the onset of condensation, and their study using the usual spectroscopic methods appears not to be easy as a result of multiple scattering of photons by atoms. This explains why, although it was first considered as a nuisance, multiple scattering is of great interest for the study of the properties of cold atoms as it is for classical scatterers. Moreover, it has also been realized that cold atoms and Bose-Einstein condensates are good candidates for the observation of coherent effects in multiple scattering not only in the weak disorder regime but also in the Anderson localization regime. Another great advantage of the resonant Rayleigh scattering of photons by atoms resides in the fact that atoms provide an almost perfect realization of point-like scatterers, an assumption that has been underlying most of our previous calculations (section A2.3.3). These various points have triggered the experimental study of the backscattering effect in cold atomic gases (Rubidium and Strontium) [236]. The behavior of the backscattering cone as a function of polarization appears to be qualitatively different from the case of classical scatterers. This shows up clearly in Figure 8.18 where the enhancement factor of the coherent albedo is much smaller in the parallel polarization channel than in the perpendicular one [237]. This is at odds with the case of classical Rayleigh (or Rayleigh-Gans) scatterers where (see sections 6.6.4 and 8.7) a scattered wave analyzed along the incident polarization channel remains unattenuated, whereas it is strongly attenuated in the perpendicular polarization channel. The reason for this unexpected behavior arises from the existence of internal atomic degrees of freedom, *i.e.*, from degenerate Zeeman sub-levels which translates into a very different expression for the elementary vertex. As for the classical Rayleigh scattering, we must consider two distinct effects. One is the depolarization of an incident photon that affects equally the Diffuson and the Cooperon, *i.e.*, the incoherent and coherent contributions to the albedo. A second effect is the decrease of the Cooperon contribution in the parallel and perpendicular polarization channels. For Rayleigh scattering by a classical dipole, this decrease occurs only in the perpendicular channel. We shall now see that for atoms with degenerate Zeeman sub-levels, it also occurs in the parallel channel (see Appendix A6.5).

- **Depolarization of the Diffuson**

The classical intensity and the incoherent albedo can be measured within either the polarization channel of the incident photons or the perpendicular channel. The characteristic dephasing times $\tau_k^{(d)}$ defined by (6.321) and presented in Table 6.22 account for the loss of polarization of an incident photon. As for Rayleigh scattering, only the scalar mode $k = 0$ survives in the long time

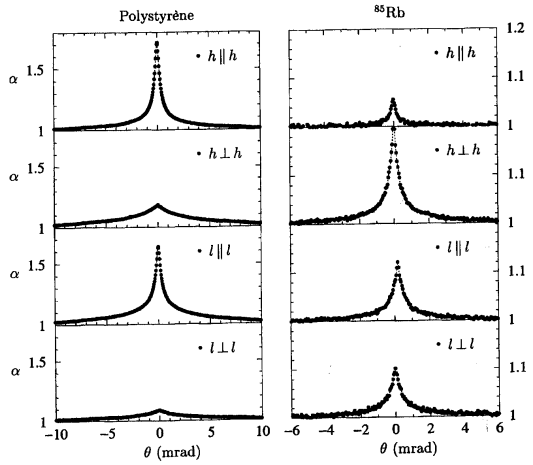

Figure 8.18: *Comparison of backscattering cones obtained for classical scatterers (polystyrene) and for cold Rubidium atoms. We notice that the enhancement factors are much smaller for atoms. Even more surprising is the behavior as a function of polarization, which differs both qualitatively and quantitatively from the classical case [236].*

limit and contributes equally in all polarization channels. Therefore, for long multiple scattering trajectories of photons, we recover the same depolarization factor 1/2 obtained in the classical case (see relation 8.58).

• Reduction of the enhancement factor of the coherent albedo

In addition to depolarization, the Cooperon involves an additional phase shift between multiple scattering amplitudes propagating in opposite directions. This phase shift gives rise to a decrease in the enhancement factor of the coherent albedo relative to the incoherent background.

For classical Rayleigh scattering (section 8.7), the scalar mode $k = 0$ of the Cooperon is a Goldstone mode. Therefore the Cooperon contribution is robust in the parallel polarization channel ($l \parallel l$ or $h \parallel h$) and it is attenuated only in the perpendicular polarization channel ($l \perp l$ or $h \perp h$). However, for atomic gases, the contribution $\Gamma_0^{(c)}(t)$ of this mode decreases exponentially since $\tau_0^{(c)}$ is now finite. Consequently, the component $\Gamma^{(c)}(t)$ of the structure factor is reduced even in the parallel channel . We may also be in a situation opposite to the classical case, *i.e.*, for which the enhancement of the coherent albedo is larger in the perpendicular channel than in the parallel one. The value of the enhancement depends on the nature of the atomic transition and on the total angular momentum of the ground state (J) and of the excited state (J_e). For instance, for Rubidium atoms, which correspond to a transition ($J = 3, J_e = 4$), we have $\tau_2^{(c)} > \tau_1^{(c)} > \tau_0^{(c)}$ (see Table 6.22). The exponential decay of the Cooperon is driven by the less rapidly decaying mode, that is by the largest time $\tau_2^{(c)}$, so that for long enough times, it decays with the same

	$\Gamma^{(d)}$	$\Gamma^{(c)}$
$l \parallel l$	$\frac{\Gamma_0^{(d)} + 2\Gamma_2^{(d)}}{3}$	$\frac{\Gamma_0^{(c)} + 2\Gamma_2^{(c)}}{3}$
$l \perp l$	$\frac{\Gamma_0^{(d)} - \Gamma_2^{(d)}}{3}$	$\frac{\Gamma_2^{(c)} - \Gamma_1^{(c)}}{2}$
$h \parallel h$	$\frac{\Gamma_0^{(d)}}{3} - \frac{\Gamma_1^{(d)}}{2} + \frac{\Gamma_2^{(d)}}{6}$	$\frac{\Gamma_0^{(c)}}{3} - \frac{\Gamma_1^{(c)}}{2} + \frac{\Gamma_2^{(c)}}{6}$
$h \perp h$	$\frac{\Gamma_0^{(d)}}{3} + \frac{\Gamma_1^{(d)}}{2} + \frac{\Gamma_2^{(d)}}{6}$	$\Gamma_2^{(c)}$

Figure 8.19: *Structure factors $\Gamma^{(d)}$ and $\Gamma^{(c)}$ in the different polarization channels as obtained from eqs. (6.323, 6.324). See exercise 2.4 and Table (2.10) for the calculation of the scalar product in the different polarization or helicity channels in the backscattering direction. For Rayleigh scattering, $\Gamma_0^{(c)} = \Gamma_0^{(d)}$ are Goldstone modes, while for scattering by Rb atoms, $\Gamma_0^{(c)}$ is attenuated and decreases faster than $\Gamma_2^{(c)}$.*

characteristic time $\tau_2^{(c)}$ in all polarization channels. Then, the height of the coherent backscattering cone $\alpha_c^{\parallel}$ in the parallel channel is comparable to that of $\alpha_c^{\perp}$ in the perpendicular channel (Figure 8.18). More quantitatively, the height of the cone in the different channels is given by the coefficient of the $k = 2$ mode which, from Table (8.19) is $2/3, 1/2, 1/6, 1$, respectively for the $l \parallel l$, $l \perp l$, $h \parallel h$ and $h \perp h$ polarization channels. This is in qualitative agreement with the results of Figure (8.18).

Finally, in the case of cold atomic gases, it is important to take into account finite size effects of the cloud that lead to a rounding of the shape of the coherent backscattering cone (Exercise 8.2). Moreover, the confinement of the atoms is achieved by means of external lasers, so that the density of the gas is non homogeneous. This raises the problem of finding the right boundary conditions for the structure factor and for the probability P_d.

8.9.4 Coherent backscattering effect in acoustics

In order to close this tour of the various systems in which coherent backscattering has been observed, let us mention the beautiful set of experiments done in acoustics [238, 239]. Figure 8.20 shows the backscattering cone for acoustic waves ($\lambda = 0.43mm$) propagating in a two-dimensional random medium of

dimensions $160mm \times 80mm$, composed of 2400 rigid steel rods immersed in a water tank. This medium is characterized by a transport mean free path $l^* \simeq 4mm$ and a diffusion coefficient $D^* \simeq 2.5mm^2/\mu s$.

The great advantage of the acoustic setup is that the detectors (a network of ultrasonic transducers) can also measure the phase of the detected signal, not only its intensity as in optics. Moreover, due to the lower speed of acoustic waves, it is also possible to have access to the time resolved behavior such as the time-dependent albedo $\alpha(\theta, t)$ defined by (8.40, 8.41). This behavior is represented in Figure 8.21. In agreement with relation (8.42), the shape of the coherent cone is Gaussian with a width that varies like $1/\sqrt{Dt}$. A similar experiment in optics would require femtosecond pulses [240].

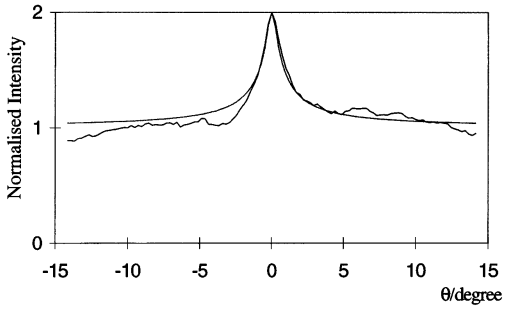

Figure 8.20: *Coherent backscattering cone measured with acoustic waves (A. Tourin et al. [239]).*

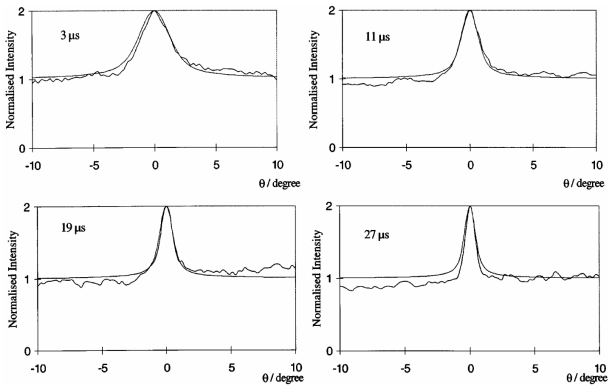

Figure 8.21: *Measurement of the time-dependent albedo $\alpha(t)$ with acoustic pulses. The cone has a Gaussian shape and its width varies like $1/\sqrt{Dt}$ (A. Tourin et al. [239]).*